Active galactic nucleus torus models and the puzzling infrared spectrum of IRAS F10214+4724

A. Efstathiou,[1]⋆ N. Christopher,[2] A. Verma,[2] R. Siebenmorgen[3]

[1]*School of Sciences, European University Cyprus, Diogenes Street, Engomi, 1516 Nicosia, Cyprus.*
[2]*Oxford Astrophysics, Denys Wilkinson Building, University of Oxford, Keble Road, Oxford OX1 3RH, UK*
[3]*European Southern Observatory, Karl-Schwarzschildstrasse 2, 85748 Garching b. München, Germany*

28 July 2018

ABSTRACT

We present a revised model for the infrared emission of the hyperluminous infrared galaxy IRAS F10214+4724 which takes into account recent photometric data from *Spitzer* and *Herschel* that sample the peak of its spectral energy distribution. We first present and discuss a grid of smooth active galactic nucleus (AGN) torus models computed with the method of Efstathiou & Rowan-Robinson and demonstrate that the combination of these models and the starburst models of Efstathiou and coworkers, while able to give an excellent fit to the average spectrum of Seyfert 2s and spectra of individual type 2 quasars measured by *Spitzer*, fails to match the spectral energy distribution of IRAS F10214+4724. This is mainly due to the fact that the νS_ν distribution of the galaxy falls very steeply with increasing frequency (a characteristic that is usually indicative of heavy absorption by dust) but shows a silicate feature in emission. Such emission features are not expected in sources with optical/near-infrared type 2 AGN spectral signatures. The *Herschel* data show that there is more power emitted in the rest-frame 20-50μm wavelength range compared with the model presented by Efstathiou which assumes three components of emission: an edge-on torus, clouds (at a temperature of 610 and 200K) that are associated with the narrow-line region (NLR) and a highly obscured starburst that dominates in the submillimetre. We present a revised version of that model that assumes an additional component of emission which we associate with NLR clouds at a temperature of 100K. The 100K dust component could also be explained by a highly obscured hot starburst. The model suggests that the NLR of IRAS F10214+4724 has an unusually high covering factor ($\geq 17\%$) or more likely the magnification of the emission from the NLR clouds is significantly higher than that of the emission from the torus.

Key words: radiative transfer - dust, extinction - galaxies: active - galaxies: individual: IRAS F10214+4724 - infrared: galaxies.

1 INTRODUCTION

The discovery paper of IRAS F10214+4724 at a redshift of 2.285 (Rowan-Robinson et al. 1991) was entitled 'An IRAS galaxy with huge luminosity - hidden quasar or protogalaxy?'. It soon became evident that gravitational lensing of a factor between 10 and 100 was responsible for the enormous luminosity that appears to exceed $10^{14} L_\odot$ (Broadhurst & Lehar 1995; Graham & Liu 1995; Serjeant et al. 1995; Eisenhardt et al. 1996). Until recently, however, it was not clear whether the dominant energy source was a quasar or a starburst. The rest-frame optical/ultraviolet (optical/UV) spectrum showed characteristics similar to that of a Seyfert

⋆ E-mail: `a.efstathiou@euc.ac.cy`

© 0000 RAS

2 (Elston et al. 1994; Lawrence et al. 1993; Goodrich et al. 1996) but the galaxy is also bright in the submillimetre suggesting the presence of an obscured starburst.

Gravitational lensing can be turned into an advantage and can help us to study in more detail an object that is at a similar redshift to large numbers of ultraluminous and hyperluminous infrared galaxies (ULIRGs and HLIRGs with luminosities exceeding 10^{12} and $10^{13} L_\odot$ respectively) that have been discovered in large surveys at far-IR and submillimetre wavelengths (e.g. PEP: Lutz et al. 2011, HerMES: Oliver et al. 2012). Recent results from such surveys suggest that high redshift ULIRGs are colder and less obscured than local ULIRGs (Rowan-Robinson et al. 2010, Elbaz et al. 2011) as suggested by radiative transfer modelling of submillimetre galaxies (Efstathiou & Rowan-Robinson 2003, Efstathiou & Siebenmorgen 2009).

A number of models for the IR spectral energy distribution (SED) of IRAS F10214+4724 were developed in the early- to mid- 1990s but they were inconclusive mainly due to the limited wavelength coverage. Rowan-Robinson et al. (1993) showed that good fits to the SED could be obtained either with a starburst or a dust embedded quasar. Green & Rowan-Robinson (1996) suggested that a combination of an active galactic nucleus (AGN) torus model and a starburst was necessary to explain the SED. Granato et al. (1996) presented a fit to the SED of IRAS F10214+4724 solely with an embedded quasar.

Mid-IR spectrophotometry has been shown to be a powerful means of differentiating between a starburst and an AGN origin of the IR emission (Roche et al. 1991 and references therin, Genzel et al. 1998, Verma et al. 2005). Starburst galaxies show mid-IR emission features that are attributed to polycyclic aromatic hydrocarbon (PAH) molecules. These features are mostly absent from the spectra of quasars (QSOs) but in general AGNs may show mid-IR emission features with smaller equivalent widths due to the mixing of the starburst and AGN torus emission (e.g. Rowan-Robinson & Efstathiou 2009). The spectra of quasars also show emission features at $10\mu m$ whereas Seyfert 2s show absorption features due to silicate dust.

In contrast, the mid-IR spectrum of IRAS F10214+4724 obtained by Teplitz et al. (2006) using the IRS onboard *Spitzer* was very puzzling as it showed an emission feature at rest frame $10\mu m$ instead of the expected absorption feature given the type 2 nature of the AGN suggested by optical observations. Efstathiou (2006; hereafter Paper I) proposed that the SED of IRAS F10214+4724 could be the combination of three components of emission: discrete clouds with a covering factor of 17% which were associated with the narrow-line region, an AGN torus viewed edge-on and a highly obscured starburst. We also noted in Paper I, however, that because the emission of the torus and the NLR clouds arises from different regions the magnification of each component may be different.

In this paper, we develop a new model for the IR emission of IRAS F10214+4724 which takes into account new photometric data from *Spitzer* and *Herschel* that cover the wavelength range 70-170μm and therefore complete its SED. In Section 2, we present the new IRAC and MIPS data. In Section 3, we discuss a recently computed grid of tapered disc models computed with the method of Efstathiou & Rowan-Robinson (1995) and a grid of starburst models computed with the method of Efstathiou, Rowan-Robinson & Siebenmorgen (2000; hereafter ERRS00). We then show that while the combination of the tapered disc and starburst models gives an excellent fit to the average spectrum of Seyfert 2 galaxies presented by Hao et al. (2007) and the spectra of type 2 QSOs (QSO2s) observed with *Spitzer*/IRS, it can not explain the SED of IRAS F10214+4724. In Section 5, we present our revised model for IRAS F10214+4724 and in Section 6 we discuss our results. A flat Universe is assumed with $\Lambda = 0.73$ and H_0=71km/s/Mpc.

2 *SPITZER* AND *HERSCHEL* OBSERVATIONS

We complemented the data from Paper I with imaging and photometry data from the *Spitzer Space Telscope* (*Spitzer*; Werner et al. 2004) Heritage Archive and data taken with the Photodector Array Camera and Spectrometer (PACS; Poglitch et al. 2010) onboard the *Herschel Space Observatory* (*Herschel*; Pilbratt et al. 2010).

IRAS F10214+4724 was observed with the Infrared Array Camera (IRAC) at 3.6, 4.5, 5.8 and 8.0 μm as part of the PRME-MISC programme (AOR: 4405248). Multiband Imaging Photometer (MIPS; Rieke et al. 2004) images were also obtained as part of the ULIRGS-GTO2 programme (AOR: 17537280) in the 70 and 160μm bands.

Imaging data from all mentioned *Spitzer* observations were used in this work, except for the MIPS 160μm, as the mosaic was of insufficient size to accurately determine the background, which contained significant structure. As Sturm et al. (2010) made a flux continuum measurement at 170μm, the lack of the 160μm constraint does not affect this work.

The Basic Calibrated images (BCD) were obtained from the Spitzer Heritage Archive, then reduced and mosaicked using the MOPEX software (version 18.4.9).

These images were corrected for geometric distortions and interpolated on to an output grid, defined by the spatial boundaries of the BCD images included in the final mosaic. The background between overlapping frames was matched and bad pixels were masked out and these pixels reinterpolated. The average of each group of input pixel values was then used to create the final mosaic image.

The IRAC BCD images were produced by the S18.18.0 version of the reduction software and calibrated according to Cohen et al. (2003). The MIPS 70μm BCDs

were produced by version S18.12.0 of the reduction software and calibrated according to Gordon et al. (2007).

Aperture photometry was then conducted to calculate the flux of IRAS F10214+4724 in the 3.6, 4.5, 5.8, 8.0 and $70\mu m$ *Spitzer* wavebands. An aperture radius of 3.6 arcsec was adopted for the IRAC mosaics and aperture corrections from the IRAC instrument handbook were applied for a background radius of 14.4-24 arcsec. No colour corrections were applied. A calibration uncertainty of 3% was implemented, as discussed in Reach et al. (2005). Possible contributions to the IRAC fluxes from the foreground lensing source were not estimated.

An aperture radius of 16 arcsec was used for the MIPS $70\mu m$ mosaic and the photometry was corrected for using aperture corrections based on the best-fitting MIPS point spread function from Gordon et al. (2008). A colour correction of 0.98 was determined according to the measured SED of IRAS F10214+4724 approximated by a power-law slope across the MIPS bands (Stansberry et al. 2007). An additional calibration uncertainty of 5% was also applied, as described in Gordon et al. (2007). Aperture sizes and aperture corrections as well as source fluxes and the associated error per *Spitzer* band are listed in Table 1.

Fluxes at 85, 108 and $170\mu m$ (observed wavelength) were obtained by PACS as part of the SHINING programme and are published in Sturm et al. (2010). These continuum fluxes were obtained from the line spectra of [OIV]$26\mu m$, [SIII]$33\mu m$ and [OIII]$52\mu m$. The PACS fluxes are also given in Table 1.

3   RADIATIVE TRANSFER MODELS

3.1   AGN torus models

When the first models for the emission of the torus in AGNs were developed (Pier & Krolik 1992, Granato & Danese 1994, Efstathiou & Rowan-Robinson 1995), the effort of these authors was mainly guided by the IRAS data and ground-based spectrophotometry in the $8-13\mu m$ window by Roche, Aitken and collaborators (Roche et al. 1991, and references therein). A spectrum of the nucleus of NGC 1068 from 2.2 to $34\mu m$ was also available (Rieke & Low 1975). The spectrophotometry showed moderate silicate absorption in Seyfert 2s and featureless spectra in Seyfert 1s. The absence of silicate emission in Seyfert 1s was very puzzling as in the context of the AGN unified scheme (e.g. Antonucci 1993) in Seyfert 1s we should be seeing the hot dust in the inner part of the obscuring torus directly and this should give rise to a silicate emission feature (Efstathiou & Rowan-Robinson 1991, Rowan-Robinson et al. 1993). Two solutions for this problem were proposed: Granato & Danese (1994) suggested that silicate dust is destroyed in the inner part of the torus by shocks. Pier & Krolik (1992) and Efstathiou & Rowan-Robinson (1995) made the torus so optically thick that it was optically thick at $10\mu m$ even when it was viewed face-on. Pier & Krolik explored the case of cylinders of constant density, whereas Efstathiou

& Rowan-Robinson that of tapered discs with a density distribution following r^{-1}. The thickness of tapered discs increases with distance from the central source in the inner part of the disc but tapers off to a constant value in the outer disc. Because of the differences in geometry and density distribution the cylindrical and tapered disc models make significantly different predictions about the emergent spectral energy distributions. The tapered discs of Efstathiou & Rowan-Robinson, in combination with the starburst models of ERRS00 have been quite successful in fitting the SEDs of a number of AGNs even in cases where mid-IR spectroscopy was available (Alexander et al. 1999, Ruiz et al. 2001, Farrah et al. 2002, Verma et al. 2002, Farrah et al. 2003, Efstathiou & Siebenmorgen 2005, Farrah et al. 2012).

More recently there has been interest in clumpy torus models (Nenkova et al. 2002, Dullemond & van Bemmel 2005, Hönig et al. 2006, Nenkova et al. 2008, Schartmann et al. 2008, Heymann & Siebenmorgen 2012, Stalevski et al. 2012) for two main reasons: first, these authors were attempting to explain the absence of silicate emission features in type 1 AGNs with clumpiness following an original suggestion by Rowan-Robinson (1995) and, secondly, theoretically it is predicted that the dust in the torus should be clumpy. The irony is that in 2005 *Spitzer* observations showed emission features in quasars and weak absorption features in Seyfert 1 galaxies (e.g. Hao et al. 2005, 2007, Siebenmorgen et al. 2005, Spoon et al. 2007). It is currently not clear whether these emission features are emitted by the torus or by NLR clouds as suggested in Paper I and by Schweitzer et al (2008). It is also not clear whether clumping of the dust in the torus is needed at all for explaining the SEDs of AGNs (see also Feltre et al. 2012).

In this paper we use a grid of tapered disc models computed with the method of Efstathiou & Rowan-Robinson (1995). In this grid of models we consider five discrete values for the equatorial 1000Å optical depth (250, 500, 750, 1000, 1250), three values for the ratio of the outer to inner disc radius r_2/r_1 (20, 60, 100) and four values for the half-opening angle of the torus Θ_0 (30°, 45°, 60° and 75°; Θ_1 as defined by Efstathiou & Rowan-Robinson is equal to $90 - \Theta_0$). The spectra are computed for 37 or 74 orientations which are equally spaced in the range 0 to $\pi/2$. The method of solution of the axially symmetric radiative transfer problem has been tested extensively and has been shown to give results that are in very good agreement with the benchmark models of Pascucci et al. (2004). The accuracy of the results is also ensured by the very good satisfaction of the flux constancy condition even in the most optically thick multi-grain models.

In Fig. 1 we show the predicted SEDs from six models that illustrate the range of spectra that can be obtained from these models. In these models, we fix the equatorial optical depth at 1000Å at 750 and vary the torus half-opening angle Θ_0 and the ratio of the outer to inner torus radius r_2/r_1. We plot the predicted spectra

Table 1. Summary of the new *Spitzer*, *Herschel*/PACS and other data for IRAS F10214+4724 which were used in the radiative transfer modelling. The listed error is the combination of the flux error and the adopted calibration uncertainty (3% of the source flux for IRAC bands and 5% for MIPS 70μm). References for the data (1) This work (2) Sturm et al. (2010) (3) IRAS (4) Benford et al. (1999) (5) Rowan-Robinson et al. (1993)

Wavelength (μm)	Flux (mJy)	Error (mJy)	Reference
Spitzer			
3.6	0.32	0.06	1
4.5	0.33	0.06	1
5.8	0.43	0.07	1
8.0	0.96	0.10	1
70.0	301	29	1
Herschel/PACS			
85	330	100	2
108	378	115	2
170	445	130	2
Other data			
60	205	45	3
350	383	51	4
450	273	45	5
800	50	5	5
1100	24	5	5

for the same inclinations in all panels for easy comparison. Most of the effects seen in Fig. 1 have been discussed in Efstathiou & Rowan-Robinson (1995) but it is useful to make some additional comments here now that we have the benefit of a larger regular grid of models. First of all, it is clear that in the face-on case we can have flat 10μm spectra as well as spectra with emission and absorption features. Secondly, for a fixed outer to inner disc radius, the anisotropy of the emission decreases with decreasing torus half-opening angle. Tori with a smaller half-opening angle emit more isotropically as they deviate less from spherical symmetry. Finally for a fixed opening angle, tori that are more extended (or, in other words, have a larger r_2/r_1) show more anisotropy in the emission. We also note that the anisotropy of the emission increases with increasing equatorial optical depth. The grid of tapered disc models, as well as the grid of starburst models discussed below, are available from AE on request (a.efstathiou@euc.ac.cy).

3.2 Starburst models

Models for the IR emission of starburst galaxies have been presented by Rowan-Robinson & Crawford (1989), Rowan-Robinson & Efstathiou (1993), Krügel & Siebenmorgen (1994), Silva et al. (1998), ERRS00, Takagi et al. (2003), Dopita et al. (2005), Siebenmorgen & Krügel (2007) and Groves et al. (2008).

The model of ERRS00, which has been updated by Efstathiou & Siebenmorgen (2009), incorporates the stellar population synthesis model of Bruzual & Charlot (1993, 2003) and involves detailed radiative transfer that takes into account absorption, emission and multiple scattering from large classical grains as well as the effect of small transiently heated grains and PAH molecules. The emission of small grains and PAHs is calculated with the method of Siebenmorgen & Krügel (1992). One distinct feature of the model is that it also incorporates a simple recipe for the evolution of the giant molecular clouds that constitute the starburst. The model predicts that by about 10 Myr after star formation, the expansion of the H_{II} region leads to the formation of a cold narrow shell of gas and dust. This naturally explains why the mid-IR spectra of starburst galaxies are dominated by the PAH emission and not by the emission of hot dust. The model predicts that as the molecular clouds evolve, their emission shifts to longer wavelengths and show stronger PAH features.

Another effect of ageing is that the clouds get more optically thin and therefore the silicate features get shallower. Once the spectra of molecular clouds at different stages in their evolution have been computed, the spectrum of a starburst at different ages can be computed by convolving the sequence of spectra with a star formation history. ERRS00 showed that the IRAS colours of starburst galaxies can be explained by a sequence of models whose star formation rate decays exponentially with an e-folding time τ of 20Myrs. The other model parameters assumed by ERRS00 (average density n_{av}, star formation efficiency η and giant molecular cloud mass M_{GMC}) were found to be in good agreement with other indicators for the starburst galaxy M82. As it is well known (e.g. Rowan-Robinson & Efstathiou 1993), ULIRGs such as Arp 220 are up to a factor of a few more
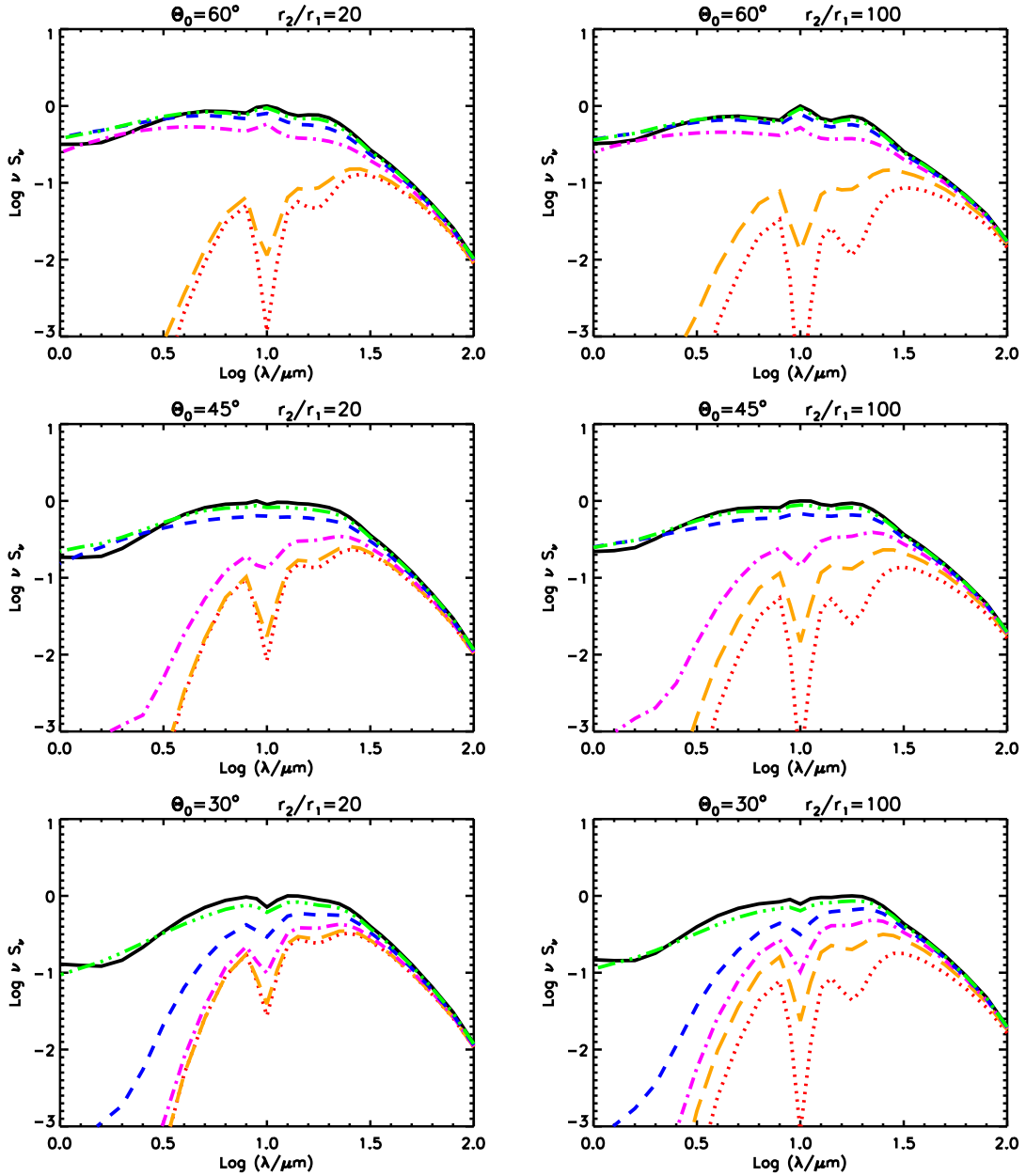
Figure 1. Predicted SEDs of tapered discs for a range of half-opening angles of the torus Θ_0 and inclinations, and two different values for the ratio of the outer to inner disc radius r_2/r_1. All models assume an equatorial optical depth at 1000Å of 750 and a density distribution that falls off as r^{-1}. We use the following code for the inclinations in all panels: red dotted line – 90°, orange dashed line – 75°, magenta dot dashed line – 60°, blue dashed line – 45°, green triple dot dashed line – 30°, black solid line – 0°,

optically thick than starbursts like M82 and NGC 1068. Verma et al. (2002) and Farrah et al. (2002) showed that the starburst models of ERRS00 in combination with the tapered discs of Efstathiou & Rowan-Robinson (1995) could explain the SEDs of HLIRGs. Farrah et al. (2003) showed that the same combination of models provided good fits to the SEDs of 41 ULIRGs. Rowan-Robinson & Efstathiou (2009) found that the same models can explain the full range of spectra measured by

the infrared spectrograph (IRS) onboard *Spitzer* (Spoon et al. 2007). One interesting prediction of the ERRS00 model is that young starbursts show strong near-IR continua, small $6.2\mu m$ equivalent widths and deep silicate absorption features and can therefore explain the galaxies in class 3A of Spoon et al. (2007). Recently Rowan-Robinson et al. (2010) found a large number of young starbursts in the HerMES project.

In this paper we use a grid of starburst models that

have been computed with the method of ERRS00 but with a revised dust model (Efstathiou & Siebenmorgen 2009) and revised stellar population synthesis models (Bruzual & Charlot 2003). We first vary n_{av}, η and M_{GMC} to give three discrete values of τ_V (50, 75 and 100) that cover the range of optical depth suggested by observations. We then compute a grid of starburst models in which we vary the age of the starburst t_* from 0 to 70Myrs in steps of 5Myr, the e-folding time of the exponentially decaying star-formation rate τ from 10 to 40Myr in steps of 10Myr and the time t_m at which the covering factor of dust reduces from 100 to 50% from 10 to 40Myr also in steps of 10Myr. This gives us a total of 720 starburst models.

3.3 Comparison with the average IR spectrum of Seyfert 2s

We first explore whether the combination of the tapered disc and starburst models described above can fit the average spectrum of Seyfert 2s presented by Hao et al. (2007). The average observed spectrum has been determined by first normalizing the spectra at rest-frame $15\mu m$ and then averaging. The *Spitzer* spectrum has been supplemented in the far-IR by determining the average IRAS fluxes of the sample of Seyfert 2s discussed by Lumsden et al. (2001) and normalizing them to the Spitzer spectrum at $12\mu m$. The tapered disc models have also been averaged in an attempt to mimic the averaging of the observed spectra. For a given AGN torus model, the predicted spectra for the relevant inclinations have been normalized at $15\mu m$ and then weighted over the viewing angle, i.e by carrying out the integral

$$\int_{i_1}^{\pi/2} \nu S_\nu(i) \ sin \ i \ di$$

where i_1 is the angle that separates a direct view of the nucleus from an obscured view.

We find that even the oldest of the starburst models considered here can not account for the average 60 and $100\mu m$ fluxes of this sample which suggests that there is a significant contribution from cold galactic discs (cirrus) to the far-IR emission. A number of the galaxies in the Lumsden et al. sample do in fact show evidence for excess $100\mu m$ emission which is indicative of cirrus. We therefore combine the starburst models with the cirrus models of Efstathiou & Siebenmorgen (2009) which assume that the diffuse galactic dust is heated by a radiation field that has the spectrum of the interstellar radiation field in the solar neighbourhood but an intensity which is a factor of ψ higher. We find that a cirrus model that has the same luminosity as the starburst and $\psi = 10$ when combined with the tapered disc models provides a very good fit to the data. The best fit to the Seyfert 2 average (shown in Figs 2 and 3) is provided by a model that assumes a torus half-opening angle of 45°, an equatorial 1000Å optical depth of 750 and a
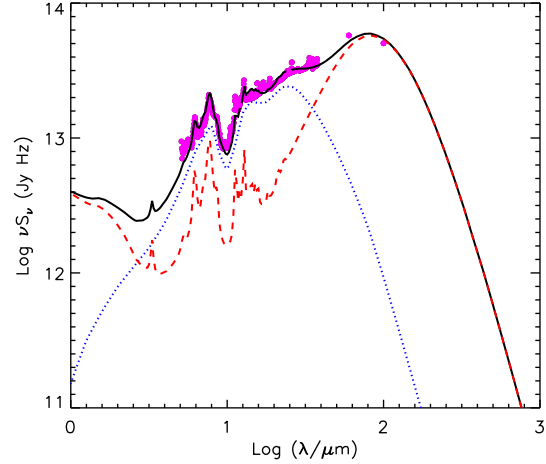

Figure 2. Fit to the average spectrum of Seyfert 2s by Hao et al. (2007). The blue dotted line gives the average emission from the AGN tapered disc model (see text) and the red dashed line the emission from the starburst/cirrus combination model (see text). The total emission is given by the solid line. The vertical scale is arbitrary.
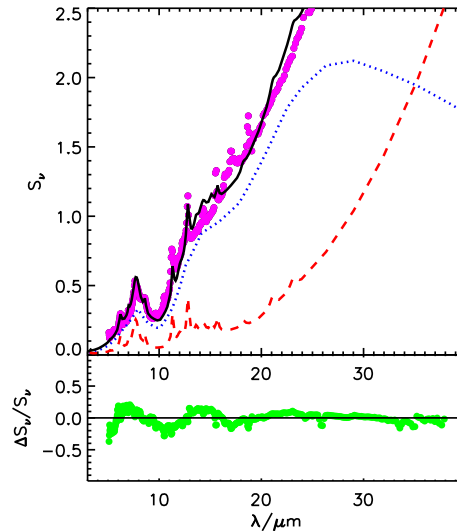
Figure 3. As Fig. 2 but showing the fit to the mid-IR spectrum on a linear scale in more detail. The vertical scale is arbitrary. The lower panel shows the residuals $(S_{model} - S_{data})/S_{data}$.

ratio of the outer to inner torus radius of 20. The best-fitting starburst model assumes $\tau_V = 100$, $t_* = 40$Myr, $\tau =$10Myr and $t_m =$10Myr.
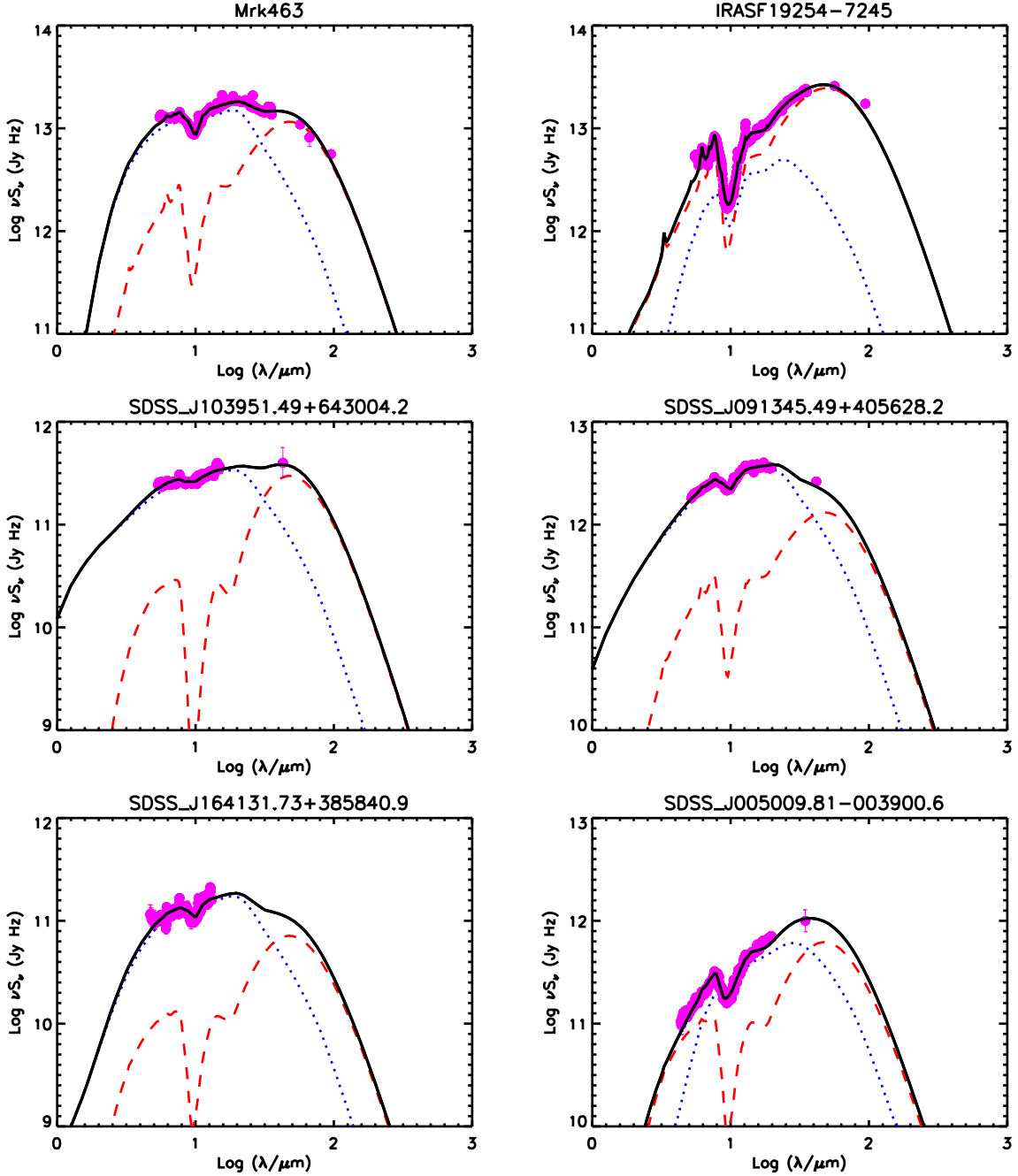
Figure 4. Best-fitting tapered disc (blue dotted) and starburst (red dashed) models for the QSOs discussed in section 4. The total emission is given by the black solid line. The best fit parameters and derived luminosities are given in Table 2. Data from Hernan-Caballero & Hatziminaoglou (2011) and IRAS.

4   COMPARISON WITH THE INFRARED SPECTRA OF QSO2S

To assess how succesful are these models in explaining the IR spectra of more luminous AGN we have compared them with the SEDs of six QSO2s from the sample of Hernan-Caballero & Hatziminaoglou (2011) which have good signal-to-noise ratio mid-IR IRS data and a range of spectral slope and apparent level of obscuration. We complement the IRS data with photometry at longer wavelengths where available. For simplicity we assume $\tau = 10$Myr and $t_m = t_*$. We find that the combination of tapered discs and starburst models presented here provide good fits to the data. The fits are shown in Fig. 4 and the best-fitting parameters and derived luminosities are given in Table 2.

Table 2. Best-fitting parameters and derived luminosities for the QSOs modelled with a combination of tapered disc and starburst models. t_* is the age of the exponentially decaying starburst, τ_V is the initial optical depth of its molecular clouds, r_2/r_1 is the ratio of the outer to inner tapered disc radius, τ_{uv}^{eq} is its equatorial UV optical depth, i is the disc inclination and Θ_0 is its half-opening angle. L_{AGN}, L_{SB} and L_{tot} are the 1-1000μm AGN, starburst and total luminosities, respectively. The AGN luminosity is corrected by the anisotropy correction factor A (Paper I).

Object name	z	t_* $(10^7 \mathrm{yr})$	τ_V	r_2/r_1	τ_{uv}^{eq}	i	Θ_0	A	$\log\frac{L_{AGN}}{L_\odot}$	$\log\frac{L_{SB}}{L_\odot}$	$\log\frac{L_{tot}}{L_\odot}$
Mrk463	0.051	0.50	50	60	250	59°	30°	1.11	11.69	11.44	11.88
IRAS F19254-7245	0.062	1.50	50	60	750	64°	45°	1.89	11.52	11.96	12.10
SDSSJ103951.49+643004.2	0.402	0.00	75	60	500	51°	45°	0.86	11.96	11.74	12.16
SDSSJ091345.49+405628.2	0.441	0.50	50	100	750	36°	30°	0.61	12.87	12.56	13.04
SDSSJ164131.73+385840.9	0.596	0.00	50	100	500	40°	30°	0.75	11.94	11.59	12.10
SDSSJ005009.81-003900.6	0.728	0.00	50	20	1250	67°	60°	4.17	13.40	12.74	13.49

The comparisons shown in this and the previous section show that existing models for starbursts, cirrus and smooth AGN tori with reasonable parameters provide good fits to the average spectrum of Seyfert 2 galaxies and spectra of individual QSO2s. The fit to the average spectrum of Seyfert 2s also shows that there is a significant contribution in the mid-IR spectra of this population by the starburst so any serious attempt to explain the *Spitzer* spectra of AGNs should consider a combination of AGN torus and starburst emission.

5   A REVISED MODEL FOR IRAS F10214+4724

We now consider whether the same combination of models can fit the SED of IRAS F10214+4724. The broadband data used in the fit are summarized in Table 1. In this analysis, we exclude the IRAC data as they require an additional starlight component to be fitted. In addition, the lensing galaxy may contribute as it is not spatially resolved from IRAS F10214+4724. We find that these models provide a very poor fit to the SED of IRAS F10214+4724 and this is shown in Fig. 5. This is clearly due to the fact that the spectrum of IRAS F10214+4724 shows an unusual combination of a silicate emission feature and weak rest-frame near-IR continuum. This suggests that the only way we could fit this spectrum with a smooth torus viewed close to edge-on is if the torus was optically thin in the mid-IR and has a maximum dust temperature of 200-300K. Such models are not included in our grid of models all of which assume a maximum dust temperature of 1000K and equatorial 1000Å optical depth in the range 250-1250. A model with a low torus optical depth is also inconsistent with the *Chandra* X-ray spectrum of F10214+4724 which suggests that if there is an AGN in this object it must be Compton-thick (Alexander et al. 2005).

A question that naturally arises from the previous discussion is: is it possible to fit the spectrum of IRAS F10214+4724 with a clumpy torus model? Nikutta et al.

(2009) presented a clumpy torus model for the SED of a type 2 quasar that shows a silicate feature in emission. In contrast to IRAS F10214+4724, this object shows a strong near-IR continuum as well. It is hard to see how even a clumpy torus with clouds as hot as 1000K viewed close to edge-on can produce a spectrum with a silicate emission feature and weak near-IR continuum. To investigate this further, we have compared the data with a combination of the clumpy torus models of Stalevski et al. (2012), which have been computed with a fully self-consistent radiative transfer code, and our starburst models. We find that the best fit, which is also shown in Fig. 5, is of similar quality to the fit obtained with the smooth torus models.

The failure of torus emission alone to fit the mid-IR SED of IRAS F10214+4724 motivated us in Paper I to propose a three-component model: an edge-on torus, clouds associated with the NLR and a highly obscured starburst. The model assumed that the NLR clouds have a covering factor of 17% and two discrete values for the dust temperature (610 and 200K). The eight-parameter fit with a model with two discrete temperatures for the NLR clouds is much more significant (reduced $\chi^2 = 2.5$) than a six-parameter fit with a model with only one temperature (reduced $\chi^2 = 11.8$). The parameters we varied are the temperature and luminosity of the two NLR components, the optical depth of the clouds, the luminosity of the starburst, the luminosity of the torus and its inclination.

We also found in Paper I that it is very difficult to fit the observed near- and mid-IR spectrum with a model that assumes that the NLR dust has a continuous distribution of dust temperature. In Fig. 8, we illustrate this by plotting the predicted spectrum of a shell of dust which has a ratio of the inner to outer radius of 0.1, a density distribution that follows r^{-1} and a total UV optical depth of 10. We assume the same grain mixture as used for the calculation of the emission of discrete clouds. The dust temperature of the shell at its inner boundary is 610K and this reduces to 73 K at the outer
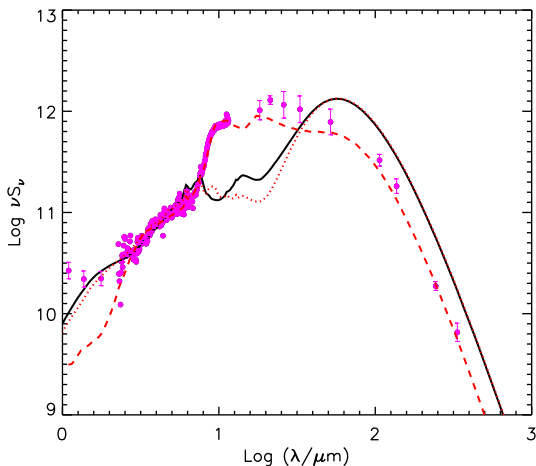
Figure 5. The solid line shows the best fit to the SED of IRAS F10214+4724 with a combination of the tapered disc models of Efstathiou & Rowan-Robinson (1995) and the starburst models of Efstathiou & Siebenmorgen (2009). Also shown as a dotted line (red) is the best fit to the data with the combination of the Stalevski et al (2012) clumpy torus models and the same starburst models. The dashed (red) line shows the fit to the data with the Paper I model. References for the data are given in Table 1.

radius. It is clear that such a model does not provide a good fit to the *Spitzer* spectrum.

The new MIPS and PACS data suggest that there is about a factor of 2 more power in the rest-frame wavelength range 20-50μm compared with the prediction of the model presented in Paper I (see Fig. 5). Considering that the new data sample the peak of the SED of IRAS F10214+4724, this implies that the covering factor needs to increase even more from an already high value. We find that the new data can be fitted by assuming an additional component of NLR dust at a temperature of 100K. The new fit is shown in Figs 6 and 7. The combination of the anisotropy of the emission of the assumed torus model ($\Theta_0 = 60^o$, $r_2/r_1 = 20$ and equatorial optical depth 1000) and the fact that the covering factor is so high makes the torus emission negligible and it is not shown in this fit. Fig. 8 shows the individual contributions from the 610, 200 and 100K dust. The luminosity of the three components is 1.4, 9.5 and $7.1 \times 10^{13} L_\odot$, respectively, giving a total apparent AGN luminosity of $1.8 \times 10^{14} L_\odot$. The starburst model assumes the same parameters as the model that provides the best fit to the Seyfert 2 average except that it is 50% more optically thick ($\tau_V = 150$). The starburst luminosity is predicted to be $6.6 \times 10^{13} L_\odot$ which is about 13% lower than that found in Paper I.

6 DISCUSSION AND CONCLUSIONS

Before we discuss the proposed model for the IR emission of IRAS F10214+4724, we would like to discuss the possibility of an alternative interpretation for the additional component that is suggested by the *Herschel* data. We have explored the possibility that this additional component is a hot starburst. To this end, we searched the data base of starburst models of Siebenmorgen & Krügel (2007) for a model that peaks in the rest-frame wavelength range 20-40μm and which is sufficiently optically thick so that its mid-IR emission does not affect the fit to the silicate emission feature which is still provided mainly by the 200K clouds.

In the starburst model of ERRS00, the luminosity of the starburst and its radius are not free parameters. A more luminous starburst is assumed to consist of more molecular clouds and the model does not specify how these clouds are distributed in space. In the starburst model of Siebenmorgen & Krügel (2007), the radius of the starburst (which is assumed to be spherical) and its luminosity are free parameters. The model also assumes that in addition to the molecular clouds that are centrally illuminated by OB stars and which constitute the so-called hot spots, there are other old bulge and massive stars that are obscured only by diffuse dust which is distributed uniformly in the starburst. The hot-spots and the free stars are distributed as $r^{-1.5}$ but the massive stars are confined to the central 350 pc. By varying the luminosity and radius of the starburst it is therefore possible to heat the diffuse dust to a high temperature of about 100K.

We find that a good fit to the complete SED can be obtained if we replace the 100 K component with a Siebenmorgen & Krügel model that assumes a luminosity of $10^{14.2} L_\odot$, a radius of 1 kpc and a visual extinction from the surface to the centre of the starburst of 119. The apparent luminosity of this component is about $7 \times 10^{13} L_\odot$ so this implies that this model is not appropriate. However, a similar spectrum could be given by a smaller starburst which is less luminous and therefore has the same dust temperature distribution.

In Paper I, it was argued that the possible reason for the appearance of a silicate feature in emission in a type 2 AGN was the dominance of the emission from the NLR clouds over the emission from an edge-on smooth torus which has a large opening angle and therefore highly anisotropic emission (Efstathiou & Rowan-Robinson 1995). Another effect that was first noted by Efstathiou, Hough & Young (1995) who modelled the nuclear IR spectrum of NGC 1068 is that if the central source of radiation is an accretion disc, the radiation directed towards the NLR may be a factor of a few more intense than the radiation directed towards the bulk of the torus. This effect was also discussed more recently by Kawaguchi & Mori (2010) who argued that the reason that the inner radius of the torus is systematically about a factor of 3 smaller than predicted from the AGN

luminosity is due to the fact that the central source is an accretion disc.

The suggestion that the silicate emission feature in a type 2 AGN is due to emission by NLR clouds also seemed to explain the fact that the average mid-IR spectrum of X-ray-selected QSO2s also showed a silicate emission feature (Sturm et al. 2006). Since then the same effect has been observed in a few Seyfert 2 galaxies, e.g. NGC 2110 (Mason et al. 2009) and a type 2 quasar (Nikutta et al. 2009). However, Martinez-Sansigre et al. (2008) and Hernan-Caballero et al. (2009) found no evidence for this effect in samples of luminous type 2 AGNs observed with the IRS onboard *Spitzer*. These results suggest that the deduced covering factor of the NLR in IRAS F10214+4724 (17% or more if the 100K emission is also from the NLR) is either unusually high or the unique spectrum is due to the preferential magnification of the emission of the NLR clouds. Mor et al. (2009) estimate that the average NLR covering factor in a sample of Palomar-Green (PG) quasars is 7%, with values as large as 42% in the case of PG 0157+001. Deane (2012) and Deane et al. (2013) have given support to the idea of preferential magnification in IRAS F10214+4724.

What is also puzzling is the fact that the observed spectrum requires the NLR dust to be concentrated in clouds with three discrete values of dust temperature instead of a continuous distribution of temperature. This may be evidence for episodic outflows of material that forms dust. Lacy, Rawlings & Serjeant (1998) also suggested on the basis of near-IR and optical spectroscopy that NLR clouds start life close to the nucleus and flow out. Alternatively, this may suggest that it is mainly the emission of the 100-200 K clouds that is preferentially magnified.

In conclusion, IRAS F10214+4724 is probably both a hidden quasar and a protogalaxy in the sense that a massive stellar population is in the process of formation at high redshift. We now find, in contrast to the predictions of the radiative transfer models of the 1990s, that the bulk of the apparent luminosity originates from the NLR. The model that came closer to the picture we now have is the 'anisotropic sphere' model of Rowan-Robinson et al. (1993) which was described in more detail by Efstathiou & Rowan-Robinson (1995). The model predicted a silicate emission feature, but its predicted near-IR continuum was too strong. The case of IRAS F10214+4724 illustrates the need for rest-frame mid-IR spectroscopy for understanding the high-redshift galaxy populations that have been uncovered by galaxy surveys at IR and submillimetre wavelengths. The case of IRAS F10214+4724 also shows that it is not at all straightforward to interpret the SEDs of objects that are gravitationally lensed. Well-sampled SEDs are needed for understanding the emission mechanisms involved and determining the fractions of luminosity that are contributed by the different components.
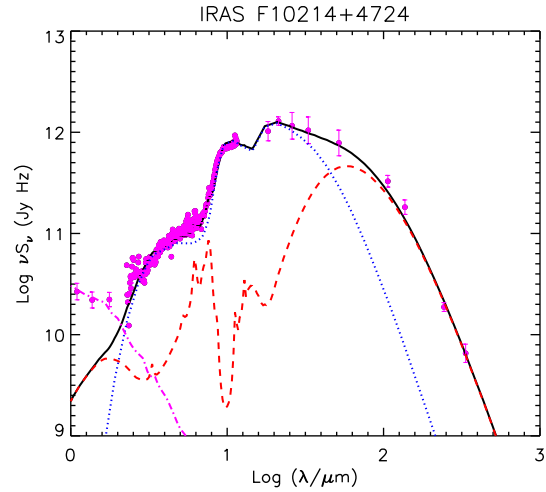

Figure 6. Fit to the SED of IRAS F10214+4724. The dotted (blue) and dashed (red) lines show the contributions of the AGN and starburst, respectively, to the total emission (solid line). The dot-dashed (magenta) line also shows a fit to the IRAC data with a 2.5-Gyr-old stellar population with a luminosity of $6.5 \times 10^{12} L_\odot$. References for the data are given in Table 1.
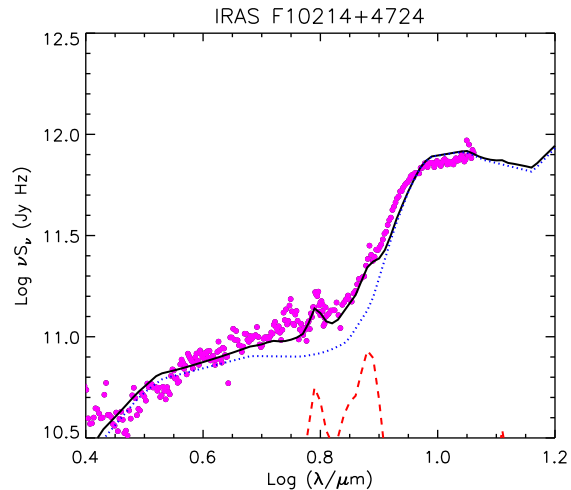
Figure 7. As Fig. 6 but showing the fit to the mid-IR spectrum in more detail.
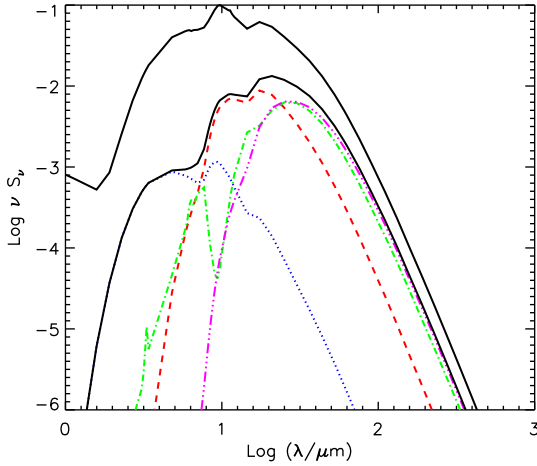
Figure 8. Spectra of the three NLR components: 610K (blue dotted line), 200K (red dashed line) and 100K (magenta triple dot-dashed line). Also shown in green (dot-dashed line) is the spectrum of the 'hot' starburst discussed in Section 5. The sum of the emission from the 610, 200 and 100K components gives the total emission from the AGN component (black solid line) which is used in the fits shown in Figs 6 and 7. Also shown with the upper black solid curve is the predicted spectrum of a shell of dust with a continuous distribution of dust and an inner dust temperature of 610K (see text for more details).

REFERENCES

Alexander, D.M., Efstathiou, A., Hough, J.H., Aitken, D.K., Lutz, D., Roche, P.F., Sturm, E. 1999, MNRAS 310, 78
Alexander, D.M., Chartas, G., Bauer, F.E., Brandt, W.N., Simpson, C., Vignali, C., 2005, MNRAS 357, L16
Antonucci, R., 1993, ARAA 31, 473
Benford, D.J., Cox, P., Omont, A.,Phillips, T.G., McMahon, R.G., 1999, ApJ 518, L65
Broadhurst, T., & Lehar, J. 1995, ApJ 450, L41
Bruzual A.G., Charlot S. 1993, ApJ 405, 538
Bruzual A.G., Charlot S. 2003, MNRAS 344, 1000
Cohen, M., Wheaton, Wm. A., Megeath, S.T., 2003, AJ 126, 1090
Deane, R., 2012, PhD thesis, Univ. of Oxford
Deane, R.P., Rawlings, S., Marshall, P.J., Heywood, I., Klckner, H.-R., Grainge, K., Mauch, T., Serjeant, S., 2013, MNRAS, 430, 2.
Dopita, M.A., et al. 2005, ApJ 619, 755
Dullemond, C.P., van Bemmel, I.M. 2005, A&A 436, 47
Efstathiou, A., 2006, MNRAS 371, L70 (Paper I)
Efstathiou A., Rowan-Robinson M. 1991, MNRAS 252, 528
Efstathiou A., Rowan-Robinson M. 1995, MNRAS 273, 649
Efstathiou, A., Hough, J.H., & Young, S. 1995, MNRAS 277, 1134
Efstathiou, A., & Rowan-Robinson, M., 2003, MNRAS 343, 322
Efstathiou A., Rowan-Robinson M., Siebenmorgen R. 2000, MNRAS 313, 734 (ERRS00)
Efstathiou, A., & Siebenmorgen, R. 2005, A&A 439, 85
Efstathiou, A., & Siebenmorgen, R. 2009, A&A 502, 541
Elbaz, D., et al., 2011, A&A 533, 119

Eisenhardt, P.R., Armus, L., Hogg, D.,W., Soifer, B.T., Neugebauer, G., Werner, M.W. 1996, ApJ 461, 72
Elston, R., McCarthy, P.J., Eisenhardt, P., Dickinson, M., Spinard, H., Januzzi, B.T., & Maloney, P. 1994, AJ 107, 910
Farrah, D., Serjeant, S., Efstathiou, A., Rowan-Robinson, M., Verma A. 2002, MNRAS 335, 1163
Farrah, D., Afonso, J., Efstathiou, A., Rowan-Robinson, M., Fox, M., Clements, D. 2003, MNRAS 343, 585
Farrah, D., et al. 2012, ApJ 745, 178
Feltre, A., Hatziminaoglou, E., Fritz, J., Franceschini, A., 2012, MNRAS 426, 120
Genzel R. et al. 1998, ApJ 498, 579
Goodrich, R.W., Miller, J.S., Martel, A., Cohen, M.H., Tran, H.D., Ogle, P.M., & Vermeulen, R.C. 1996, ApJ 456, L9
Gordon, K.D., et al., 2007, PASP 119, 1019
Gordon, K.D., et al., 2008, ApJ 682, 336
Graham, J.R., & Liu, M.C. 1995, ApJ 449, L29
Granato G.L., Danese L. 1994, MNRAS 268, 235
Granato, G.L., Danese, L., & Franceschini, A. 1996, ApJ 460, L11
Green, S., & Rowan-Robinson, M. 1996, MNRAS 279, 884
Groves, B., Dopita, M.A., Sutherland, R.S., Kewley, L.J., Fischera, J., Leitherer, C., Brandl, B., van Breugel, W., 2008, ApJS 176, 438
Hao, L., et al. 2005, ApJ 625, L75
Hao, L., et al. 2007, ApJ 655, L77
Heymann, F., & Siebenmorgen, R., 2012, ApJ 751, 27
Hernan-Caballero, A., et al. 2009, MNRAS 395, 16
Hernan-Caballero, A., Hatzimanaoglou, E., 2011, MNRAS 414, 500
Hönig, S.F., Beckert, T., Ohnaka, K., Weigelt, G., 2006, A&A 452, 459
Kawaguchi, T., & Mori, M., 2010, ApJ 724, L183
Krügel E., Siebenmorgen R., 1994 A&A 282, 407
Lacy, M., Rawlings, S., Serjeant, S. 1998, MNRAS 299, 1220
Lawrence, A., et al. 1993, MNRAS 260, 28
Lumsden, S., Heisler, C.A., Bailey, J.A., Hough, J.H., Young, S., 2001, MNRAS 327, 459
Lutz, D., et al., 2011, A&A 532, L10
Martinez-Sansigre, A., Lacy, M., Sajina, A., Rawlings, S., 2008, ApJ 674, 676.
Mason, R. E., Levenson, N. A., Shi, Y., Packham, C., Gorjian, V., Cleary, K., Rhee, J., and Werner, M., 2009, ApJ 693, L136.
Mor, R., Netzer, H., Elitzur, M., 2009, ApJ, 705, 298.
Nenkova M., Ivezic Z., Elitzur M. 2002, ApJ 570, L9
Nenkova, M., Sirocky, M.M., Nikutta, R., Ivezic, Zeljko, Elitzur, M., 2008, ApJ 685, 160
Nikutta, R., Elitzur, M., Lacy, M., 2009, ApJ 707, 1550
Oliver et al., 2012, MNRAS 424, 1614
Pascucci, I., et al. 2004, A&A 417, 793
Pier E. A., Krolik J. H. 1992, ApJ 401, 99
Pilbratt, G.L., et al. 2010, A&A 518, L1
Poglitch, A., et al. 2010, A&A 518, L2
Reach, W.T., et al., 2005, PASP 117, 978
Rieke, G.H., et al. 2004, ApJS 154, 25
Rieke, G.H., Low, F.J., 1975, ApJ 199, L13
Roche P.F., Aitken D.K., Smith C.H., Ward M.J. 1991, MNRAS 248, 606
Rowan-Robinson, M., 1995, MNRAS 272, 737
Rowan-Robinson M. Crawford J. 1989 MNRAS 238, 523
Rowan-Robinson, M., Efstathiou, A. 1993, MNRAS 263, 675
Rowan-Robinson, M., et al. 1991, Nature 351, 719
Rowan-Robinson M. et al. 1993, MNRAS 261, 513

Rowan-Robinson, M., & Efstathiou, A., 2009, MNRAS 399, 615

Rowan-Robinson, M., et al., 2010, MNRAS 409, 2

Ruiz, M., Efstathiou, A., Alexander, D.M., Hough, J. 2001, MNRAS 325, 995

Schartmann, M., et al., 2008, A&A 482, 67

Schweitzer, M., et al., 2008, ApJ 679, 101

Serjeant, S., Rawlings, S., Lacy, M., McMahon, R.G., Lawrence, A., Rowan-Robinson, M., & Mountain, M. 1995, MNRAS 298, 321

Siebenmorgen, R., & Krügel, E. 1992, A&A 259, 614

Siebenmorgen, R., Hass, M., Krügel, E., Schulz, B. 2005, A&A 436, L5

Siebenmorgen, R., & Krügel, E., 2007, A&A 461, 445

Silva L., Granato G. L., Bressan A. & Danese L. 1998, ApJ 509, 103

Spoon, H.W.W., et al., 2007, ApJ 654, L49

Stalevski, M., Fritz, J., Baes, M., Nakos, T., Popovic, L.C., 2012, MNRAS 420, 2756

Stansberry, J.A., et al. 2007, PASP 119, 1038

Sturm, E., Hasinger, G., Lehmann, I., Mainieri, V., Genzel, R., Lehnert, M.D., Lutz, D., & Tacconi, L.J. 2006, ApJ 642, 81

Sturm, E., et al. 2010, A&A 518, L36

Tagaki, T., Arimoto, N., Hanami, H., 2003, MNRAS 340, 813

Teplitz, H.I. et al. 2006, ApJ 638, L1

Verma A., Rowan-Robinson M., McMahon R., Efstathiou A. 2002, MNRAS 335, 574

Verma, A., Charmandaris, V., Klaas, U., Lutz, D., Haas, M., 2005, Space Sc. Rev. 119, 355

Werner, M.W., et al., 2004, ApJS 154, 309